Periodica Polytechnica Electrical Engineering and Computer Science, 69(2), pp. 198–206, 2025

Bandwidth Enhancement of a Current Sensing Trace by Adaptive Inverse Filtering

Ákos Ferenc Hegedűs[1*], Tamás Dabóczi[1]

[1] Department of Artificial Intelligence and Systems Engineering, Faculty of Electrical Engineering and Informatics, Budapest University of Technology and Economics, Műegyetem rkp. 3., H-1111 Budapest, Hungary
[*] Corresponding author, e-mail: hegedus43akos@yahoo.com

Received: 16 November 2024, Accepted: 20 February 2025, Published online: 27 February 2025

Abstract

In our previous article we proposed a novel current measurement technique, the CSRTRI (Current Sensing by Real-Time Resistance Identification), which is characterized by the main principle of the in-situ identification of the current rail's resistance by an auxiliary inductive coil in the face of continuously varying conductor-temperature. The feasibility of the method was shown, and an accuracy of 0.93%...1.10% was demonstrated. The accuracy is limited by the stray inductance of the Cu-trace, which in combination with the resistance forms a temperature dependent highpass filter. We introduced an analog RC-lowpass filter based compensation method at 25°C nominal temperature and reached a bandwidth of 2 MHz. In this paper, we present an adaptive digital inverse filtering based compensation method instead. The advantage of this approach is that it covers the whole temperature range of the sensor, not just a narrow nominal value. The enhancement does not require any additional temperature sensor; we will utilize the instantaneous estimate of the copper trace's resistance from the CSRTRI-algorithm directly to identify the cutoff frequency of the parasitic highpass filter in situ, without the need to determine the copper temperature itself. A temperature dependent time-varying first order lowpass filter of approximately 48 kHz cutoff frequency is applied to eliminate the main inductive overshoots. By this software-based transfer function enhancement a 1.5 MHz overall system bandwidth has been achieved between 20°C and 50°C conductor-temperature.

Keywords

current, current control, current measurement, digital signal processing, inductive coupling, inductive transducers, instruments, inverse filtering, resistive transducers, sensor, sensor fusion, sensor systems and applications

1 Introduction

Humanity's pursuit of global sustainability requires maximizing the efficiency of electric energy generation, transmission, and utilization [1]. Therefore, it is of utmost importance to monitor the flow of electric energy from power plants, through the power grid, to the consumers as well, as to optimize its ultimate utilization [2]. The most pivotal part of electric power measurement is the current sensing, thus the importance of low cost, high bandwidth, high accuracy current sensors has increased significantly in recent decades.

Shunts: The most widespread type of such current sensing devices is the shunt, which is used to convert the current I into a voltage signal U through its resistance R following Ohm's law: $U = I \cdot R$. Shunts have excellent bandwidth (2 GHz or higher) and accuracy (1% or better) facilitated by their negligible TCR (thermal coefficient of resistance) and optional Kelvin-contacts [3, 4]. For maximal system-efficiency and minimal temperature rise the shunt's $P_{loss} = U \cdot I$ power dissipation needs to be reduced, necessitating lower voltage signal levels [5, 6]. In high power applications the indispensable galvanic isolation, significant self-heating and cost are the typical disadvantages of shunts.

Hall Sensors: Magnetic field based current sensing is most frequently realized by ICs with integrated Hall-cells [7]. This method leverages the $U_{Hall} = R_H \cdot I_{bias} \cdot B_z/d$ Hall-voltage signal, which is proportional to the B_z out-of-plane magnetic field component of the current. Here the R_H parameter is called the Hall-coefficient, I_{bias} is the bias current, and d the thickness of the Hall-plate. Hall-sensors usually reach an overall accuracy of 2-3%, when piecewise calibrated over temperature. They have inherent galvanic isolation and extremely low insertion resistance, enabling their practical and cost-effective application in the high power segment. Their bandwidth spans typically DC to 100 kHz, but in some cases as high as a few MHz could be

Cite this article as: Hegedűs, Á. F., Dabóczi, T. "Bandwidth Enhancement of a Current Sensing Trace by Adaptive Inverse Filtering", Periodica Polytechnica Electrical Engineering and Computer Science, 69(2), pp. 198–206, 2025. https://doi.org/10.3311/PPee.38815

reached [8–13]. Modest speed and accuracy, in comparison to other methods, are the main drawbacks of this approach.

Magnetoresistance: As an alternative to Hall-cells, DC-capable magnetoresistive current sensors like TMR (Tunneling Magnetoresistance) utilize a magnetic tunnel junction thin film's resistance-dependence on magnetic field. TMR current sensors can achieve a bandwidth of 1 MHz and an accuracy of 1% [14, 15].

ICS (Inductive Current Sensors): Another widespread current measurement principle is based on the Law of Induction, i.e., the Faraday Effect. ICSs comprise a sensing-coil, positioned close to the primary conductor and a voltage signal is induced proportional to the time-derivative of the current's magnetic field according to Maxwell's 3rd equation. Since according to Maxwell's 4th equation, the induced magnetic field is proportional to the primary current, for the induced voltage we get $U_{ind} = M \cdot dI/dt$. Here M denotes the mutual inductance between the conductor and the coil, dI/dt indicates the slope of the current. Therefore, ICSs are completely insensitive to DC-currents. U_{ind} may be integrated by an amplifier stage, to get a voltage output, proportional to the current signal. ICSs are distinguished by their inherent galvanic isolation, zero insertion resistance and excellent upper bandwidth. Overall, ICSs are the optimal choice for high voltage, high power AC-current measurement. Specific ICS-manufacturers offer off-the-shelf current probes characterized by $f_{min,-3\ \mathrm{dB}} = 1$ Hz and $f_{max,-3\ \mathrm{dB}} = 200$ MHz cutoff frequencies [16–18].

In CTs (current transformers), a sort of ICSs, the primary current is converted to a secondary current by transformer action, which is then measured through a precision resistor.

2 CSRTRI (Current-Sensing through real-time Resistance Identification)

The idea to utilize the ohmic resistance of a conductor element, like a PCB-copper trace, similarly to a shunt, for current measurement, arises intuitively [19]. With appropriate dimensioning the required DC-resistance value can be set:

$$R = \frac{\rho \cdot l}{w \cdot d}. \tag{1}$$

Here ρ is the resistivity of the metal, l denotes the trace's length, w its width, d its thickness. Beside a fixed R value one might increase both l and w, to improve the cooling. Unfortunately, one runs into some difficulties when trying to implement the concept. Due to the trace's L self-inductance, its impedance can be modelled as $Z \approx R + j\omega L$ with good approximation. Here R itself increases significantly over frequency because of the skin effect. Both phenomena can be largely suppressed by antiparallel design shown by Fig. 1, which minimizes L and the magnetic field through the conductor's surface, hence the skin effect also.

The residual highpass filter-like frequency characteristics may be largely eliminated by additional analog RC-lowpass filtering at a specific Cu-temperature. Whereas initial uncertainties of R, caused by manufacturing tolerances, can be overcome by piecewise EOL-calibration, abrasion and corrosion may also alter the resistance in the long run. Primarily, ρ shows a significant thermal drift for metals other than shunt alloys, thereby R increases strongly over T. More specifically, the TCR of annealed copper is $\alpha_{Cu} = 3930$ ppm/K, which implies a large T-dependence both due to varying ambient temperature and self-heating. The resultant dynamic resistance variation can only be partially compensated by direct on-trace T-sensing [20–22]. This large in-situ variation of R renders accurate current measurement directly via a copper-trace impossible, despite its considerable voltage signal. As a solution to this problem, we proposed the CSRTRI method for PWM-controlled systems in [1]. Here the R-value, being continuously evaluated by the microprocessor, combined with a high bandwidth U_R trace voltage measurement, enables excellent accuracy. The main principle of the CSRTRI is the following: let us place a coil near a current trace of resistance R, so that the mutual inductance between the trace and the coil is M. By having a differential-coil arrangement homogeneous background field suppression can be achieved (Fig. 2).

For a current waveform $I = I(t)$ we can write the following equations for the voltage signals:

$$U_R = R \cdot I, \tag{2}$$

$$U_M = M \cdot \frac{dI}{dt} \equiv M \cdot \dot{I}. \tag{3}$$

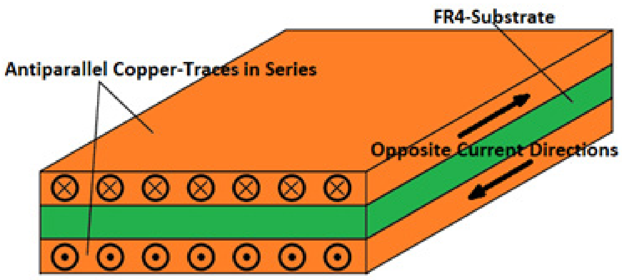

Fig. 1 Low-inductance, PCB-based, current-conductor design

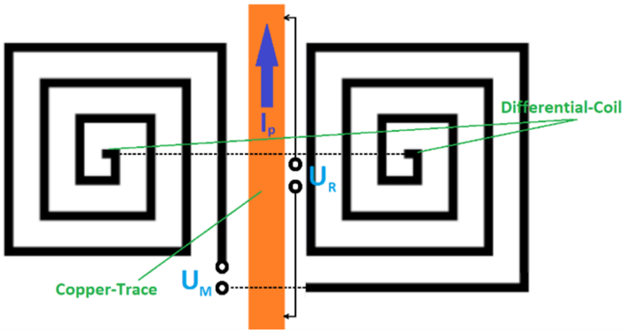

Fig. 2 Visualization of the CSRTRI concept

Here U_R denotes the output voltage of the resistive trace, U_M is the induced voltage of the coil, $\dot{I}$ is the time-derivative of the current. Let us take the time derivative of Eq. (2):

$$\dot{U}_R = \dot{R} \cdot I + R \cdot \dot{I} \tag{4}$$

As detailed in [1], in practical PWM-controlled systems, the first term in Eq. (4), $\dot{R} \cdot I$ is negligible:

$$\dot{U}_R \approx R \cdot \dot{I}. \tag{5}$$

Excluding the case of the pure, ideal DC-current, i.e., $\dot{I} \neq 0$, we may divide the Eq. (5) by (3):

$$\frac{\dot{U}_R}{U_M} \approx \frac{R \cdot \dot{I}}{M \cdot \dot{I}} = \frac{R}{M}. \tag{6}$$

It means that in effect we can identify the actual resistance value in-situ, by dividing the time derivative of the resistor's voltage by the coil's induced voltage at any point in time, and multiplying the quotient by the practically temperature-independent mutual inductance value, supposing first, that the noise is negligible:

$$R(t) \approx M \cdot \frac{\dot{U}_R(t)}{U_M(t)}. \tag{7}$$

The pure $\dot{U}_R$ and U_M signals differ only in a slowly drifting scaling-factor according to Eq. (6). Having preliminary information on the signal spectrum, for example by knowing the PWM-frequency, the application of the appropriate digital bandpass filter on both signals $\dot{U}_R$ and U_M, leaves their ratio unchanged, while the SNR (Signal to Noise Ratio) of the R-identification, shown by Eq. (7), can be largely improved. In our concrete implementation, we applied a sliding window to calculate the DFTs of the acquired waveform-segments recursively, to realize a highly selective digital bandpass filter exactly at the PWM-frequency, f_0:

$$\begin{aligned}\hat{R}(t_0) &= M \cdot \frac{\dot{U}_R(t_0,\tau) * h_{BP}(t)}{U_M(t_0,\tau) * h_{BP}(t)} \\ &= M \cdot \frac{\{DFT(\dot{U}_R)\}(f) \cdot H_{BP}(f)}{\{DFT(U_M)\}(f) \cdot H_{BP}(f)} \\ &= M \cdot \frac{\{DFT(\dot{U}_R)\}(f_0)}{\{DFT(U_M)\}(f_0)},\end{aligned} \tag{8}$$

where $*$ denotes convolution, $\{DFT(U)\}(f)$ denotes the discrete Fourier transform (DFT) of signal $U(t_0, \tau)$. To speed up the algorithm we calculated only the f_0 component of the DFT. To further improve SNR, we applied a median filter to $\hat{R}(t)$, which resulted in $R_{median}(t)$. Finally, as shown by the flow chart in Fig. 3, we calculated the actual $I(t)$ from Ohm's law and compared it against the reference signal of a precision-shunt, $I_{ref}(t)$:

$$I(t) \approx \hat{I}(t) = \frac{U_R(t)}{R_{median}(t)} \tag{9}$$

To validate our CSRTRI-method, we excited our system with a unipolar triangle-like current waveform, including both significant AC- and DC-content, and acquired the raw voltage signal waveforms: the $U_{shunt}(t)$ shunt-voltage, the resistive $U_R(t)$ signal of the Cu-trace, and the inductive $U_M(t)$ signal of the differential-coil for 5ms time and f_0 = 2 kHz fundamental ripple-frequency, for copper-temperatures from 16.9°C to 62.1°C. For this relatively low signal frequency, the stray inductance effect is negligible, thus no highpass filter-like behavior is observable in $U_R(t)$. Fig. 4 depicts $\hat{R}(t)$

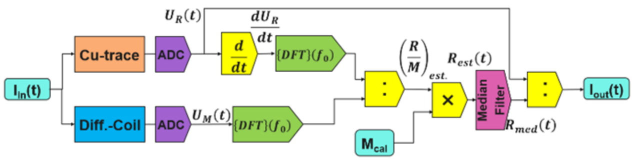

Fig. 3 Flow chart illustrating the CSRTRI implementation

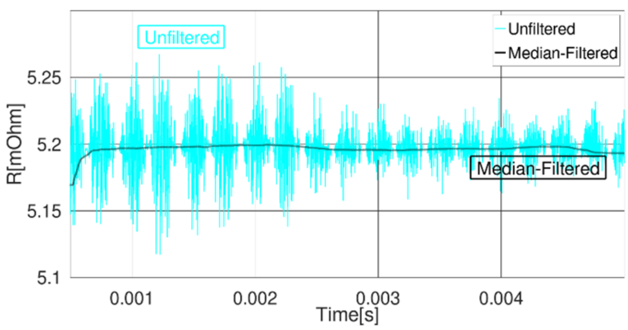

Fig. 4 Trace-resistance identification for triangle-like current excitation of f_0 = 2 kHz and T_{Cu} = 62.1°C [1]

and $R_{median}(t)$, Fig. 5 the measured $I(t)$ and $I_{ref}(t)$ waveforms at $T_{Cu} = 62.1$°C and their differences over time, i.e., the current measurement error on separate panes. The latter one consists mainly of noise, and has an RMS-value, which is 0.93% ... 1.10% of the whole current signal's RMS-value.

3 Identification of the impedance model parameters

3.1 The applied impedance models

First, we measured the $R_{Cu,25°C}$ resistance of the Cu-trace via the four-point probes method, in the same way as described in [1], to eliminate lead- and contact resistances. For our actual setup, from five measurement rounds we got $R_{Cu,25°C} = (4.895 \pm 0.004)\,\text{m}\Omega$ for 25°C.

As mentioned in Section 2, due to the self-inductance of the Cu-trace, an additional inductive term shall be considered in its impedance. Further parasitic effects resulting from the trace's stray capacitance are considerable only in the higher frequency (HF) range typically above several MHz, thus we neglected them in our approximate impedance model:

$$Z_{Cu}\left(j\omega\right) = R_{Cu} \cdot \left(1 + j\omega / \omega_{Cu}\right) \tag{10}$$

where $\omega_{Cu} = R_{Cu}/L_{Cu}$ is the angular cutoff frequency, R_{Cu} is the resistance, L_{Cu} is the self-inductance of the Cu-trace. Since R_{Cu} is strongly temperature-dependent, as already discussed, so is ω_{Cu}, however L_{Cu} can be considered practically independent of T. Determining $R_{Cu} = R_{median}$ by the RTRI method, ω_{Cu} can also be calculated adaptively:

$$Z_{Cu}\left(j\omega\right) = R_{median} \cdot \left(1 + j\omega L_{Cu} / R_{median}\right) \tag{11}$$

One shall divide $U_R \equiv U_{Cu}$ by $Z_{Cu}(j\omega)$ instead of purely considering $R_{Cu} = R_{median}$ when calculating the actual current by Eq. (9) to enhance the CSRTRI's frequency characteristics, and hence to increase the overall bandwidth.

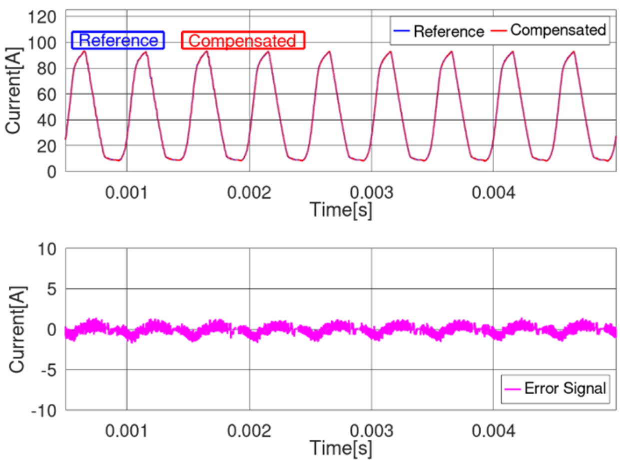

Fig. 5 Current measurement validation at $f_0 = 2$ kHz and $T_{Cu} = 62.1$°C [1]

This is equivalent of inverse filtering the U_R voltage signal by $(1 + j\omega\tau)^{-1}$, where $\tau = \omega_{Cu}^{-1}$, and dividing it by R_{median}, as shown by Fig. 6. The more accurate the calculated $Z_{Cu}(j\omega)$ using Eq. (11) is, the more ideal the current measurement's transfer function will be. It is important to emphasize, that $R_{Cu} = R_{median}$ and consequently $\omega_{Cu} = R_{median}/L_{Cu}$ in Eqs. (10) and (11), vary over temperature, so they are time-variant parameters. Still, due to the RTRI-algorithm, R_{median} and ω_{Cu} are continuously being calculated during operation, so they can be updated in situ. We used a 2512-size SMD-shunt of $R_{sh} = 8$ mΩ resistance and ±0.5% tolerance as a reference in the present work. According to the shunt's datasheet its TCR is within ±75 ppm/K [23], which is negligible compared with the TCR of the Cu-trace. We verified both R_{sh} and the TCR beside varying temperature between 24°C and 63°C. We got $R_{sh} = (8.028 \pm .004)$ mΩ and $|TCR_{sh}| < 20$ ppm/K for the concrete part, which we applied.

Anyhow, the shunt is prone to behave as an inductive impedance too, because of its smaller, still nonzero L_{sh} stray-inductance. To sum up, the shunt's impedance over ω can be expressed as:

$$Z_{sh}\left(j\omega\right) = R_{sh} \cdot \left(1 + j\omega / \omega_{sh}\right) \tag{12}$$

where $\omega_{sh} = R_{sh}/L_{sh}$ is the shunt's angular cutoff frequency. Since R_{sh} and L_{sh} are temperature-invariant with good approximation, so is $Z_{sh}(j\omega)$.

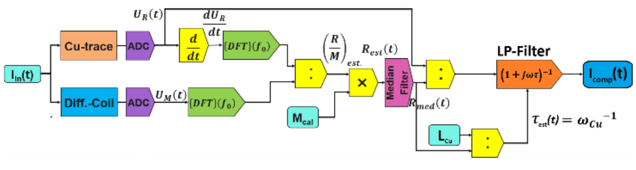

Fig. 6 CSRTRI flow chart with the time-variant inverse-filtering

3.2 The test setup

To determine the raw transfer function of the Cu-trace by identifying its impedance model parameters, and to validate the results, we decided to apply current pulses of different slopes, magnitude (approximately 500 A to 600 A) and 20 µs length both to the copper-trace and to the 8 mΩ SMD-shunt connected in series. To that end we connected a 10 mF electrolytic capacitor to a Basetech BT-3010 power supply through an 11 Ω precharge-resistor. The role of the capacitor was to be the source of the fast current pulses, so we connected the shunt, the sensor-PCB including the Cu-trace and an IRF1405 power MOSFET to it, in series, as shown by Fig. 7. Since the purpose of this setup was to achieve an eligible SNR at HF also, the current had to be switched on and off quickly, thus the dI/dt current slope had to be large.

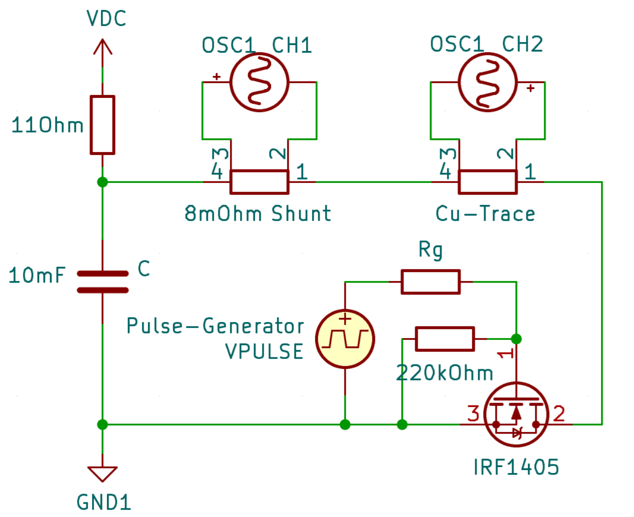

Fig. 7 The low inductance test-setup, including current pulse generator, reference shunt and Cu-trace

To minimize the arising *L dI/dt* inductive voltage overshoot at switch-off, the whole circuit had to be shrunk to the minimum size reachable. The current itself was switched by a Hameg HM8035 20 MHz pulse generator connected to the gate of the IRF1405 power MOSFET. The pulse generator itself was triggered through its external trigger input by a Hameg HM8030-5 function generator with a 40 mHz square wave signal, i.e., once every 25 seconds. In the parameter identification phase, we connected the pulse generator output directly to the MOSFET's gate to reach the steepest possible pulse-signal edges, hence the widest possible spectrum. In the validation phase afterwards, we applied R_{g1} = 470 Ω and R_{g2} = 940 Ω alternately beside the direct connection, i.e., R_g = 0 for the sake of different current slopes, and ultimately test-signal diversity. Since the input capacitance of the IRF1405 is C_{iss} = 5.48 nF, the resulting additional time constants in the gate control circuit were $\tau_1 = R_{g1} \cdot C_{iss}$ = 2.58 µs and $\tau_2 = R_{g2} \cdot C_{iss}$ = 5.15 µs respectively. We refer to the generated current-pulses with R_g = 0 as square pulses, whereas with R_{g1} and R_{g2} the waveform stimuli are called triangle pulses. We used a PicoScope 3206 PC Oscilloscope of 200 MHz bandwidth to acquire the $U_{shunt}(t)$ shunt-voltage, and the $U_{Cu}(t)$ trace voltage signals.

Considering purely the ohmic parts of the Cu-trace's and the shunt's impedance, i.e. R_{Cu} in Eq. (10) and R_{sh} in Eq. (12), and applying Ohm's law simply to the acquired raw voltage waveforms, one gets the uncompensated current waveforms, which include significant dynamic measurement errors, i.e. apparent over- and undershoots due to the stray inductances in the first place. These raw, unfiltered current signals for two different current slopes are shown by Figs. 8 and 9.

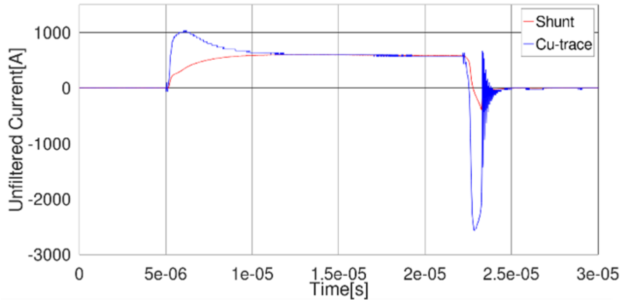

Fig. 8 Unfiltered current waveforms (T_{Cu} = 20.0°C, R_g = 0 Ω)

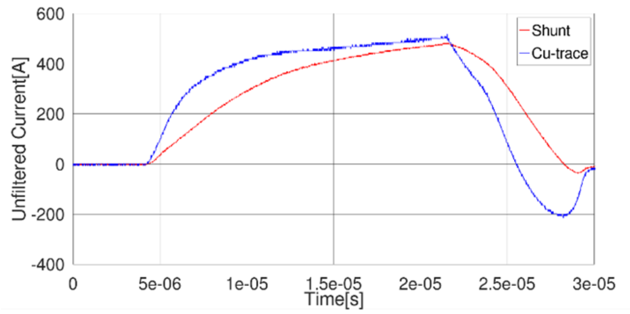

Fig. 9 Unfiltered current waveforms (T_{Cu} = 20.5°C, R_g = 940 Ω)

3.3 The parameter identification method and results

To identify the parameters of $Z_{sh}(j\omega)$ and $Z_{Cu}(j\omega)$, we measured and analyzed the impulselike-response of the trace at different temperatures. The shunt was connected in series with the Cu-trace, and they were excited with a non-ideal square pulse of roughly 600 A amplitude, 20 µs length and spectrum $I(j\omega)$, as described in the previous subsection.

Acquiring the trace's $U_{Cu}(t)$ and the shunt's $U_{sh}(t)$ voltage signals simultaneously, applying Ohm's law to them in the Fourier-space, for the measured transfer function we can write:

$$H(j\omega) = \frac{U_{Cu}(j\omega)}{U_{sh}(j\omega)} = \frac{I(j\omega) \cdot Z_{Cu}(j\omega)}{I(j\omega) \cdot Z_{sh}(j\omega)} = \frac{Z_{Cu}(j\omega)}{Z_{sh}(j\omega)} \tag{13}$$

Substituting Eqs. (10) and (12) to Eq. (13), we get:

$$H(j\omega) = \frac{R_{Cu} \cdot (1 + j\omega / \omega_{Cu})}{R_{sh} \cdot (1 + j\omega / \omega_{sh})} \tag{14}$$

First, we determined the unknown parameters (R_{Cu}, ω_{Cu} and ω_{sh}) by means of frequency domain system identification of $H(j\omega)$. (R_{sh} = 8.028 mΩ with good accuracy, independent of temperature.) For that, we used the FDIDENT toolbox of Matlab [24].

Frequency domain identification has the advantage that model fitting can be accomplished based on selected DFT points of input/output spectra. On that way we could omit spectral parts with poor SNR in the model fitting. Based on the first couple of trials we expect the ω_{Cu} zero around 300 krad/s and the ω_{sh} pole at 1.7 Mrad/s (i.e., 48 kHz and 270 kHz respectively). Thus, we selected the low frequency part (from DC up to 650 kHz) of the raw Frequency Response Function and fitted a continuous time parametric model in $j\omega$ domain of order 1/1, as shown by Fig. 10. In this frequency band, ω_{Cu} and ω_{sh} are expected to have the dominant effects on the transfer function. This way we got the best fitting model parameters for the lower frequency range.

Second, we determined the optimal model parameters by a roaming-based optimum search in the parameter-space, making use of the following inverse-filtering formulae:

$$I(j\omega) = \frac{U_{Cu}(j\omega)}{Z_{Cu}(j\omega)} = \frac{U_{Cu}(j\omega)}{R_{Cu} \cdot (1 + j\omega / \omega_{Cu})} \tag{15}$$

$$I_{ref}(j\omega) = \frac{U_{sh}(j\omega)}{Z_{sh}(j\omega)} = \frac{U_{sh}(j\omega)}{R_{sh} \cdot (1 + j\omega / \omega_{sh})} \tag{16}$$

The main principle here is the variation of R_{Cu}, ω_{Cu} and ω_{sh} as inverse-filter parameters in Eqs. (15) and (16), with the goal of minimizing the RMS-value of the current measurement error $I_{err}(t) = I(t) - I_{ref}(t)$.

We repeated the model fitting with the two above methods for several measurements at different temperatures. To this end we increased the temperature of the Cu-trace and the whole setup homogeneously under a transparent cover, using an IR-lamp before the excitation by the square current pulse. Since R_{sh} and L_{sh} are practically T-invariant, and so is ω_{sh}, we calculated the most likely value of ω_{sh} according to both fitting methods, and as a result, we got ω_{sh} = 1710 krad/s in good agreement, which is equivalent to $L_{sh} = R_{sh}/\omega_{sh}$ = 4.69 nH. This fits the 5 nH value specified in [23] well.

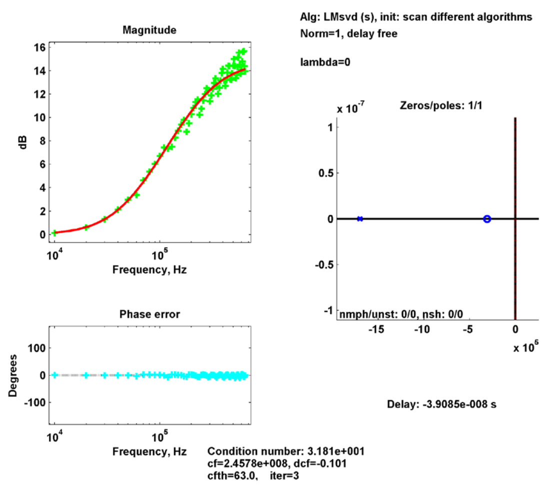

Fig. 10 Fitting of R_{Cu}, ω_{Cu} and ω_{sh} by FDIDENT

Considering, that $R_{Cu} = \omega_{Cu} \cdot L_{Cu}$ where L_{Cu} is practically independent of T, R_{Cu} and ω_{Cu} shall increase in direct proportion expectedly as the temperature increases. The actual obtained R_{Cu} and ω_{Cu} parameters over T are shown by Table 1. We plotted R_{Cu} over ω_{Cu} for both methods and fitted the datapoints applying a linear function according to $R_{Cu} = \omega_{Cu} \cdot L_{Cu}$, to get L_{Cu} directly as the slope of the resultant regression lines, as shown by Fig. 11.

The frequency domain identification resulted $L_{Cu,1} \approx$ 15.80 nH, slightly lower than the roaming algorithm in the inverse filter parameter space, which gave $L_{Cu,2} \approx$ 16.04 nH each beside $R^2 = 1$, i.e. essentially perfect fit. Although $L_{Cu,1}$ is supposed to be more reliable in terms of describing the system's behaviour in the sub-MHz region by more accurately identifying the stray inductance, we decided to choose $L_{Cu} = L_{Cu,2}$ for our inverse-filter, to achieve the lowest possible RMS-error in the impulse-like-response. The explanation is that by overcompensating the physical stray inductance by roughly 1.5%, parasitic higher order effects significant above 1 MHz, like that of the stray capacitances, are somewhat better mitigated.

Table 1 Parameter-identification results

Method	FDIDENT		ROAMING	
T_{Cu} [°C]	R_{Cu} [mΩ]	ω_{Cu} [krad/s]	R_{Cu} [mΩ]	ω_{Cu} [krad/s]
23.8	4.882	309.2	4.870	303.7
22.9	4.851	307.0	4.855	303.1
22.5	4.829	306.3	4.847	302.5
22.3	4.826	305.8	4.843	301.8
21.6	4.817	304.1	4.830	300.3
32.2	5.017	317.1	5.034	315.7
32.6	5.028	317.3	5.041	314.3
32.4	5.012	317.5	5.037	314.1
45.3	5.242	332.5	5.286	328.7
46.4	5.267	334.0	5.307	330.0

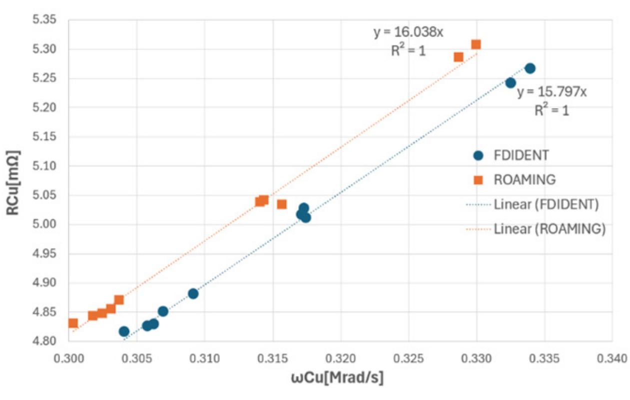

Fig. 11 Direct proportionality of R_{Cu} to ω_{Cu}

The actual conductor-temperature, T_{Cu} was calculated from the fitted R_{Cu}, using the Cu-trace as its own temperature-sensor practically making use of the copper's known TCR:

$$R_{Cu} = R_{Cu,25°C} \cdot \left(1 + \alpha_{Cu} \cdot \left(T_{Cu} - 25°C\right)\right) \tag{17}$$

Because of the direct proportionality between R_{Cu} and ω_{Cu}, the cutoff angular frequency shall show basically the same temperature dependence as the trace resistance. We got $\alpha_{Cu,fitted} \approx 3938$ ppm/K back as the slope of the fitted trendline in good agreement with the theoretical value.

4 Compensation by inverse filtering

During operation, the RTRI-algorithm is continuously updating R_{Cu}, and since L_{Cu} = 16.04 nH is known and constant, $\omega_{Cu} = R_{Cu}/L_{Cu}$ can also be refreshed in parallel. As a result, similarly to Eq. (9), the current calculation may take place through the inverse filtering formula of Eq. (15). We applied a finite difference method in the time domain to implement Eq. (15) numerically in case of the measured impulses. The effect of the inverse filtering is illustrated by Fig. 12. We summarized our results in Table 2. In average, a relative RMS-error of 1.50% has been achieved with respect to the impulselike-responses. The measured and thereafter inverse filtered current waveforms are depicted by Figs. 13 and 14. The negative undershoot of up to 20 A observable in the I_{ref} primary current after switch-off is the consequence of the oscillation of the parasitic series LC circuit.

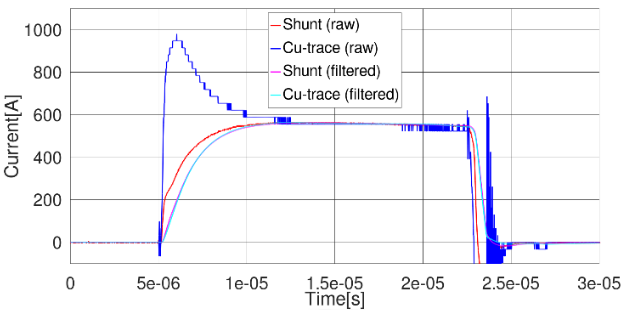

Fig. 12 Effect of inverse filtering (T_{Cu} = 22.9°C, R_g = 0 Ω)

Table 2 Validation results

#	R_g [Ω]	T [°C]	I_{rms} [A]	ΔI_{rms} [A]	$\Delta I_{rms}/I_{rms}$
1	0	20.0	326	5.13	1.57%
2	0	22.9	312	4.21	1.35%
3	0	32.4	339	4.97	1.47%
4	0	46.4	350	5.63	1.61%
5	470	19.9	307	4.54	1.48%
6	470	19.3	303	4.43	1.46%
7	940	20.5	238	3.66	1.54%
8	940	20.4	238	3.54	1.49%

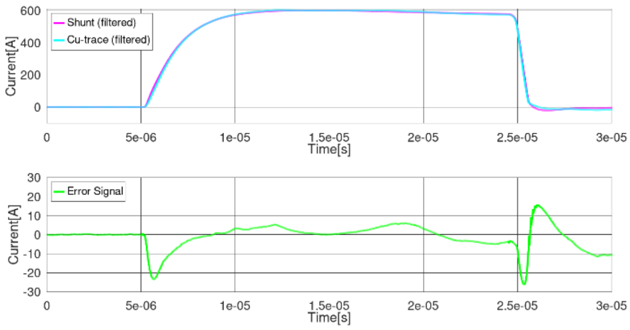

Fig. 13 Inverse-filtered response to square pulse (T_{Cu} = 46.4°C, R_g = 0 Ω)

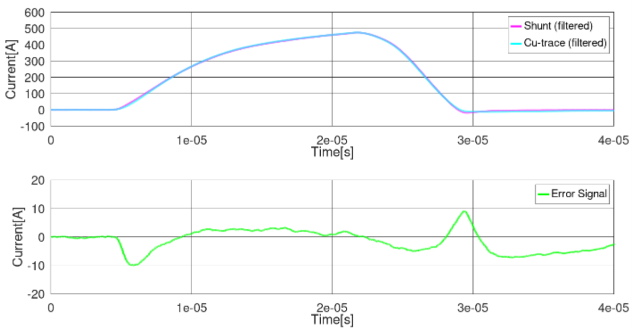

Fig. 14 Inverse-filtered response to triangle pulse (T_{Cu} = 20.5°C, R_g = 940 Ω)

Fig. 15 depicts the dominant effect of the temperature adaptivity of our inverse filtering technique on the dynamic current measurement error.

By dividing the spectra of the output and input currents and smoothing the resultant raw transfer function's absolute value, we could calculate the −3 dB bandwidth, and we got 1.5 MHz as a result, as shown by Figs. 16 and 17.

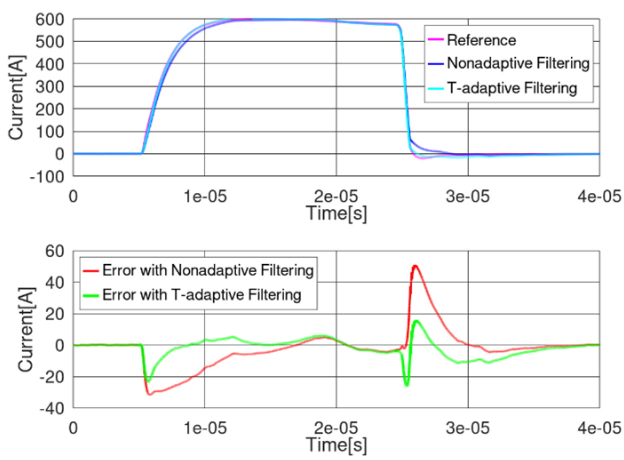

Fig. 15 Effect of T-adaptivity on impulse-response (T_{Cu} = 46.4°C, R_g = 0 Ω)

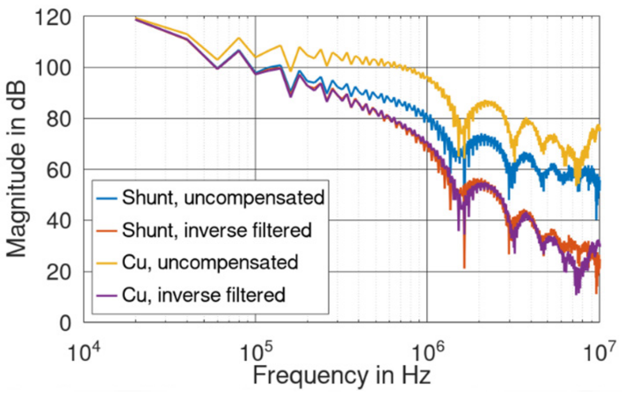

Fig. 16 Inverse filtered signal spectra (T_{Cu} = 46.4°C, R_g = 0 Ω)

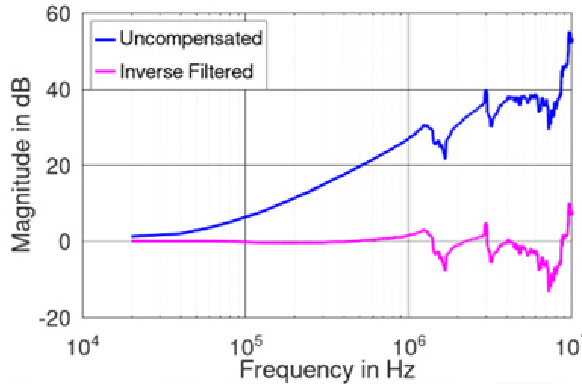

Fig. 17 Resultant transfer function (T_{Cu} = 46.4°C, R_g = 0 Ω)

5 Conclusion

Through the presented temperature-variant digital inverse filtering technique a typical 1.5% RMS-current error and a −3dB bandwidth of 1.5 MHz was reached for conductor temperatures ranging from 20°C to 50°C. This method, combined with the RTRI, has the potential to make an adaptive, in-situ stray inductance effect compensation of the CSRTRI-based current measurement feasible, even considering significant temperature variations.

Acknowledgement

T. Dabóczi acknowledges the financial support of Project no. RRF-2.3.1-21-2022-00009, titled National Laboratory for Renewable Energy, provided by the Recovery and Resilience Facility of the European Union within the framework of Program Széchenyi Plan Plus.

References

[1] Hegedűs, Á. F., Dabóczi, T. "A Wideband Current Sensing Method Based on Real-Time Resistance Identification", IEEE Transactions on Instrumentation and Measurement, 73, 9500314, 2024. https://doi.org/10.1109/TIM.2023.3338684

[2] Elma, O., Ozdemir, S., Selamogullari, U. S. "Analyzing the effect of inverter efficiency improvement in wind turbine systems", In: International Conference on Renewable Energy Research and Application (ICRERA), Milwaukee, WI, USA, 2014, pp. 572–575. ISBN: 978-1-4799-3795-0 https://doi.org/10.1109/ICRERA.2014.7016449

[3] Zhang, W., Zhang, Z., Wang, F., Brush, E. V., Forcier, N. "High-Bandwidth Low-Inductance Current Shunt for Wide-Bandgap Devices Dynamic Characterization", IEEE Transactions on Power Electronics, 36(4), pp. 4522–4531, 2021. https://doi.org/10.1109/TPEL.2020.3026262

[4] Braudaway, D. W. "Behavior of resistors and shunts: with today's high-precision measurement capability and a century of materials experience, what can go wrong?", IEEE Transactions on Instrumentation and Measurement, 48(5), pp. 889–893, 1999. https://doi.org/10.1109/19.799641

[5] Nelson, A., Pratheesh, G., Afzal, M., Navaneeth, N. K., Zhang, W., Zhang, Z. "Isolated Current Shunt and Voltage Measurement for Motor Drives Using AM437x", [pdf] Texas Instruments Incorporated, Dallas, TX, USA, 2015. Available at: https://www.ti.com/lit/ug/tidu755/tidu755.pdf [Accessed: 10 March 2023]

[6] Vogel, K., Gadermann, M., Schmal, A., Urban, C. "System Cost Reduction with Integration of Shunts in Power Modules in the Power Range above 75 kW", In: PCIM Europe 2018; International Exhibition and Conference for Power Electronics, Intelligent Motion, Renewable Energy and Energy Management, Nuremberg, Germany, 2018, pp. 1–7. ISBN: 978-3-8007-4646-0

[7] Motz, M., Ausserlechner, U., Bresch, M., Fakesch, U., Schaffer, B., Reidl, C., Scherr, W., Pircher, G., Strasser, M., Strutz, V. "A miniature digital current sensor with differential Hall probes using enhanced chopping techniques and mechanical stress compensation", In: SENSORS, 2012 IEEE, Taipei, Taiwan, 2012, pp. 1–4. ISBN: 978-1-4577-1767-3 https://doi.org/10.1109/ICSENS.2012.6411161

[8] Asahi Kasei Microdevices "High-Speed Response Coreless Current Sensor", [pdf] AKM, Tokyo, Japan, 2021. Available at: https://www.akm.com/content/dam/documents/products/current-sensor/cq3300/cq3300-en-datasheet.pdf [Accessed: 11 March 2023]

[9] Jouyaeian, A., Fan, Q., Motz, M., Ausserlechner, U., K. A. A. Makinwa, K. A. A. "5.6 A 25A Hybrid Magnetic Current Sensor with 64mA Resolution, 1.8MHz Bandwidth, and a Gain Drift Compensation Scheme", In: 2021 IEEE International Solid- State Circuits Conference (ISSCC), San Francisco, CA, USA, 2021, pp. 82–84. ISBN: 978-1-7281-9549-0 https://doi.org/10.1109/ISSCC42613.2021.9365767

[10] Funk, T., Groeger, J., Wicht, B. "An Integrated and Galvanically Isolated DC-to-15.3 MHz Hybrid Current Sensor", In: 2019 IEEE Applied Power Electronics Conference and Exposition (APEC), Anaheim, CA, USA, 2019, pp. 1010–1013. ISBN: 978-1-5386-8330-9 https://doi.org/10.1109/APEC.2019.8722098

[11] Allegro Microsystems "ACS370: 1 MHz Bandwidth, Galvanically Isolated Current Sensor", [online] Available at: https://www.allegromicro.com/en/Products/Sense/Current-Sensor-ICs/Zero-To-Fifty-Amp-Integrated-Conductor-Sensor-ICs/ACS730 [Accessed: 11 March 2023]

[12] Crescentini, M., Marchesi, M., Romani, A., Tartagni M., Traverso, P. A. "A Broadband, On-Chip Sensor Based on Hall Effect for Current Measurements in Smart Power Circuits", IEEE Transactions on Instrumentation and Measurement, 67(6), pp. 1470–1485, 2018.
https://doi.org/10.1109/TIM.2018.2795248

[13] Crescentini, Ramilli, R., Gibiino, G. P., Marchesi, M., Canegallo, R., Romani, A., Tartagni, M., Traverso, P. A. "The X-Hall Sensor: Toward Integrated Broadband Current Sensing", IEEE Transactions on Instrumentation and Measurement, 70, 2002412, 2021.
https://doi.org/10.1109/TIM.2020.3036764

[14] Helmuth Lemme "The Universal Current Sensor", [online] Available at: https://www.fierceelectronics.com/components/universal-current-sensor [Accessed: 12 March 2023]

[15] Crocus Technology "TMR Coreless Current Sensing in EVs", [online] Available at: https://crocus-technology.com/tmr-coreless-current-sensing-in-evs/ [Accessed: 12 March 2023]

[16] Pearson Electronics "Wide Band Current Monitors", [online] Available at: https://pearsonelectronics.com [Accessed: 12 March 2023]

[17] Wang, J., Hedayati, M. H., Liu, D., Adami, S.-E., Dymond, H. C. P., Dalton, J. J. O., Stark, B. H. "Infinity Sensor: Temperature Sensing in GaN Power Devices using Peak di/dt", In: 2018 IEEE Energy Conversion Congress and Exposition (ECCE), Portland, OR, USA, 2018, pp. 884–890. ISBN: 978-1-4799-7312-5
https://doi.org/10.1109/ECCE.2018.8558287

[18] Votzi, H. L., Vogelsberger, M. A., Ertl, H. "Low-Cost Current Sensor for Power Capacitors Based on a PCB Rogowski-Coil", In: 2011 PCIM Europe, Nuremberg, Germany 2011, pp. 621–626. ISBN: 978-3-38007-3344-6

[19] Ziegler, S., Woodward, R. C., Iu, H. H.-C., Borle, L. J. "Investigation into Static and Dynamic Performance of the Copper Trace Current Sense Method", IEEE Sensors Journal, 9(7), pp. 782–792, 2009.
https://doi.org/10.1109/JSEN.2009.2021803

[20] Ziegler, S., Iu, H. H.-C., Woodward, R. C., Borle, L. J. "Theoretical and practical analysis of a current sensing principle that exploits the resistance of the copper trace", In: 2008 IEEE Power Electronics Specialists Conference, Rhodes, Greece, 2008, pp. 4790–4796. ISBN: 978-1-4244-1667-7
https://doi.org/10.1109/PESC.2008.4592730

[21] Weßkamp, P., Melbert, J. "High Performance Current Measurement with Low-Cost Shunts by means of Dynamic Error Correction", In: 18. GMA/ITG-Fachtagung Sensoren und Messsysteme 2016, Nürnberg, Germany, 2016, pp. 224–230. ISBN: 978-3-9816876-0-6
https://doi.org/10.5162/sensoren2016/3.4.4

[22] Dumcius, A., Augutis, V., Gailius, D. "The modeling of temperature field in the sensor zone", In: ITI 2008 - 30th International Conference on Information Technology Interfaces, Cavtat, Croatia, 2008, pp. 691–696. ISBN: 978-953-7138-12-7
https://doi.org/10.1109/ITI.2008.4588495

[23] Vishay Intertechnology "Power Metal Strip® Resistors, Very High Power (to 3 W), Low Value (Down to 0.0005 Ω), Surface-Mount", [pdf] Vishay Intertechnology, Malvern, PA, USA, 2024. Available at: https://www.vishay.com/docs/30122/wslp.pdf [Accessed: 13 October 2024]

[24] Budapesti Műszaki és Gazdaságtudományi Egyetem (BME), Villamosmérnöki és Informatikai Kar (VIK), Mesterséges Intelligencia és Rendszertervezés Tanszék "Frequency Domain System Identification Toolbox for Matlab: Tools for frequency domain model identification and validation", [online] Available at: https://home.mit.bme.hu/~kollarzs/fdident/ [Accessed: 13 October 2024]